Synthesis and Properties of *S. Cerevisiae*-based Bionanocomposite

Boyce Ang Kok Hong (Hong Guo Feng), Sun Zizhuo

Group 01-06

Abstract

Heavy metal ions, dyes and oils are contaminants that pose serious threats to human health and the ecosystem. Different methods of removing these contaminants have been employed but have negative side effects. Therefore, biosorbents, including *S. Cerevisiae* have been used to remove contaminants in wastewater, as they are readily available and have large sorption sites without the disadvantages of current methods. Furthermore, coating biomaterial with magnetite, a non-toxic, non-carcinogenic and chemically stable material, gives it paramagnetic properties for easy removal. Hence, this study aims to synthesise and evaluate the properties of yeast-based bionanocomposites (YB-MNP) in their ability to remove contaminants such as Cu^{2+}, Fe^{3+}, Zn^{2+}, direct red 80 (DR80), methylene blue (MB), methyl orange (MB) and diesel from wastewater. Characterization of both yeast biomass (YB) and YB-MNP were conducted to determine participating functional groups in the removal of contaminants, their point of zero charge as well as their isotherm adsorption mechanism. YB performed significantly better in the removal of Fe^{3+}, Zn^{2+} and MB while performing marginally better in the adsorption of MO. YB-MNP significantly outperformed YB in the adsorption of Cu^{2+} and DR80. Both YB and YB-MNP showed no significant adsorption of diesel. It is hence concluded that YB-MNP is a promising candidate for removing select heavy metal ions and dyes which can offer key insights into the development of wastewater treatment.

1. Introduction

When contaminated wastewater enters the environment, it threatens human health and the ecosystem. One of these contaminants is heavy metal ions. They are non-biodegradable and may be carcinogenic. Cu^{2+}, Zn^{2+} and Fe^{3+} ions have been found in tap water in Dhahran, Saudi Arabia due to the corrosion of pipe materials and coatings (Sadig and Alam, 1989). If present in water in improper amounts, they can cause serious health problems for living organisms and should be removed from wastewater (Qasem et al., 2021). Another contaminant would be dyes. Industry activities, especially the textile sector, cause dyes to leach into water streams, negatively affecting living life (Karisma et al., 2017).

Furthermore, dye wastewater production has increased year by year, and due to the complex compositions of dyes, it is difficult to biodegrade in high concentrations and colour (Liu, 2020). The final contaminant would be oils. Annually, 2.7 million litres of oil are spilt into the seas, contaminating waters, killing organisms and causing lasting damage to ecosystems and economies (Bandera, 2023).

Different cleaning methods have been employed for oil spills but have negative side effects. Dispersants increase the solubility of organic compounds in water, such as polycyclic aromatic hydrocarbons, which leads to increased mutagenesis rates (Allan et al., 2012; Paul et al., 2013). Hence, biosorbents have been used to remove synthetic and natural oils from water, as biomaterials are readily available, produced on a large scale, and have large sorption sites (Carrilho et al., 2002; Labuto et al., 2018). Nanomaterials have also been extensively researched due to their high capacity to remove wastewater contaminants (Nassar, 2010). Coating yeast with magnetite nanoparticles gives it paramagnetic properties for easy removal (Yu et al., 2015), and unlike dispersants, magnetite nanoparticles are also believed to be non-toxic, non-carcinogenic, and chemically stable (Stokinger, 1984).

2. Objectives and Hypotheses

This study was conducted to investigate the rates of adsorption of heavy metal ions (Cu^{2+}, Fe^{3+} and Zn^{2+}), dyes (direct red 80, methylene blue and methyl orange) and oil (diesel), by both yeast-based bionanocomposite (YB-MNP) and *S. Cerevisiae* yeast biomass (YB). This aimed to investigate if coating yeast biomass with magnetite improved its adsorption capabilities.

It was hypothesised that *S. Cerevisiae* biomass could be prepared which can then be magnetised to produce S. *Cerevisiae*-based magnetic bionanocomposites. It is also hypothesised that YB-MNP and YB show different rates of heavy metal ion, dye and oil adsorption and that the rate of adsorption by YB-MNP would be greater than YB.

3. Materials and Methods

3.1 Growth of *S. Cerevisiae* yeast biomass (YB)

Yeast Peptone Dextrose (YPD) broth was prepared to comprise 1% yeast extract, 2% glucose, and 2% peptone. *S. Cerevisiae* yeast was precultured and upscaled in YPD broth, in an incubator

shaker for 24 h at 30°C each. The yeast was then centrifuged and washed with deionised water, then absolute ethanol. Yeast biomass was obtained after drying and stored for future use.

3.2 Synthesis of magnetite (Fe_3O_4)

A solution of 7.8 g of $FeCl_3 \cdot 6H_2O$ was mixed with a solution of 3.8 g of $FeSO_4 \cdot 7H_2O$. A 2.0 M NaOH solution was added dropwise into the above solution until the pH was raised to 10-11 to precipitate Fe_3O_4. Fe_3O_4 nanoparticles were separated using a neodymium magnet and washed repeatedly with deionised water till pH neutral. The magnetite was dried in a hot air oven and crushed in mortar and pestle before storage.

3.3 Synthesis of yeast-based bionanocomposite (YB-MNP)

YB and magnetite were suspended in deionised water in mass proportion 1:8. The suspension was heated to 80°C and stirred vigorously for 30 minutes. The suspension was dried and the YB-MNP formed was stored.

3.4 Characterisation of YB, Fe_3O_4 and YB-MNP

A Bruker Alpha FT-IR spectrophotometer obtained YB, Fe_3O_4 and YB-MNP FTIR spectra. Fe_3O_4 and YB-MNP were analysed using a scanning electron microscope (SEM).

The point of zero charge (PZC) of a biomass is when the net surface charge is 0. 0.01 g of YB and YB-MNP were each suspended in 5 mL pH 2-12 solutions, adjusted using 0.100 mol dm^{-3} HC*l* and NaOH and measured using a pH meter. The tubes were then shaken in an orbital shaker for 72 hours. The graph of final pH against initial pH and the graph of initial pH were plotted on the same axes. The PZC was determined when the change in pH reached zero, i.e. the graph of final pH against initial pH intersects the graph of initial pH.

3.5 Preparation of heavy metal ion and dye solutions

0.197 g of $CuSO_4 \cdot 5H_2O$, 0.362 g of $Fe(NO_3)_3 \cdot 9H_2O$ and 0.220 g of $ZnSO_4 \cdot 7H_2O$ were each dissolved in 1 L of deionised water. The concentration of each solution was then determined using a colourimeter.

0.050 g of direct red 80, methylene blue and methyl orange were each dissolved in 1 L of deionised water. 5 different solutions of each dye solution were prepared using different ratios of dye solution to deionised water n:10, where $n \in \{1, 0.8, 0.6, 0.4, 0.2\}$. Calibration curves for

each dye were determined by first measuring wavelength absorption using a UV-VIS spectrophotometer – 526 nm for direct red 80, 664.5 nm for methylene blue and 463.5 nm for methyl orange. Then, the graph of wavelength absorption/abs against dilution ratio was plotted. Its R^2 value and equation were then found, as seen in figures S1 to S3.

3.6 Removal of heavy metal ions and dyes with YB and YB-MNP

For each heavy metal ion and dye, 5 sets of 0.1 g of YB and YB-MNP were suspended in 10 mL of solution in a centrifuge tube each. The centrifuge tubes were shaken in an orbital shaker for 2 hours. Each centrifuge tube was taken out in 30-minute intervals and centrifuged before a sample was taken out. Then, the concentration of each sample was determined. The average concentration of each interval was plotted on a graph of concentration/ppm against time/min.

3.7 Removal of diesel by YB and YB-MNP

5 sets of 0.1 g of YB were suspended in 10 mL of diesel in a centrifuge tube. The centrifuge tubes were shaken in an orbital shaker for 30 minutes. The mass, m_{beaker}, of each of the six beakers was measured, and a filtration setup was set up. Each of the centrifuge tubes was filtered at the same time, along with 10 mL of diesel as the control setup. After all the oil had been filtered through each setup, the mass of each beaker with oil, m_{final}, was determined. The mass of oil filtered by each setup, m_{oil}, is determined: $m_{oil} = m_{final} - m_{beaker}$, while the average mass filtered, $m_{average}$, was found. The percentage mass of oil adsorbed would be $\%m_{adsorbed} = \frac{m_{average}}{m_{control}} \times 100\%$. This procedure was repeated for YB-MNP.

3.8 Isotherm Studies

Langmuir and Freundlich isotherms were originally used for gas-phase adsorption but have been adopted to correlate adsorption equilibria in heavy metal and dye adsorption. The Langmuir isotherm is given in the following form,

$$\frac{1}{Q_e} = \frac{1}{C_e}\left(\frac{1}{K_b A_s}\right) + \frac{1}{A_s}$$

, where Q_e (in mg/g) is the biosorption capacity at equilibrium while C_e is the equilibrium concentration (in mg/L). By plotting the graph of $\frac{1}{Q_e}$ against $\frac{1}{C_e}$, the maximum adsorption amount of the adsorbent, A_s, and the Langmuir constant representing the energy of adsorption,

K_b, was found through the gradient and intercept respectively. K_b was also used to determine the suitability of the biosorbent for the adsorbate, utilising Hall's separation factor, R_L, represented as

$$R_L = \frac{1}{1+K_b C_0}$$

, where C_0 is the initial concentration of the solution (Dahiya et al., 2008). R_L can be interpreted as follows, such that

$R_L < 0$, unfavourable; $R_L > 1$, unfavourable; $0 < R_L \leq 1$, favourable; $R_L = 0$, irreversible.

The Freundlich isotherm is given in the following form,

$$log\ Q_e = \frac{1}{n} log\ C_e + log\ K_f$$

, where Q_e (in mg/g) is the biosorption capacity at equilibrium while C_e is the equilibrium concentration (in mg/L). By plotting the graph of log Q_e against log C_e, the constant indicating adsorption capacity, n, and the constant indicating adsorption capacity, K_f, were found through the gradient and intercept respectively.

4. Results and Discussion

4.1 Calibration curves for dyes

The relationship between wavelength absorption, λ_{abs}, and n (and subsequently, concentration), was derived. A high R^2 value (>0.99) suggests that the model is a good fit for the data given.

4.2 FTIR spectra of YB and YB-MNP

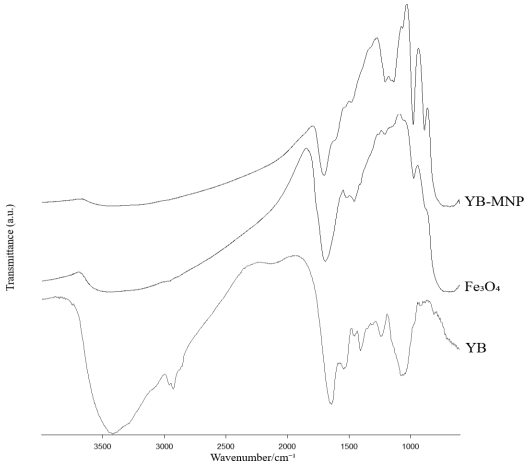

Figure 1. FTIR spectra of YB-MNP, Fe_3O_4 and YB.

Based on the FTIR spectra (Figure 1), magnetite (Fe_3O_4) was successfully synthesised as indicated by the peak at 573.71 cm^{-1}, which corresponds to Fe–O stretching. The main groups in YB were notably present, including C–C at 1069.26 cm^{-1}, P=O at 1241.76 cm^{-1}, O–C=O at 1406.59, C=O at 1641.29 cm^{-1} and –OH and $–NH_2$ stretching at 3425.18 cm^{-1}. Similar peaks were also observed in YB-MBP, notably with P=O and O–C=O functional groups either reduced or absent. An extra peak at 585.12 cm^{-1} showed the presence of Fe–O, and therefore YB-MNP was successfully synthesised.

4.3 Scanning electron microscope (SEM) analysis of Fe_3O_4 and YB-MNPb

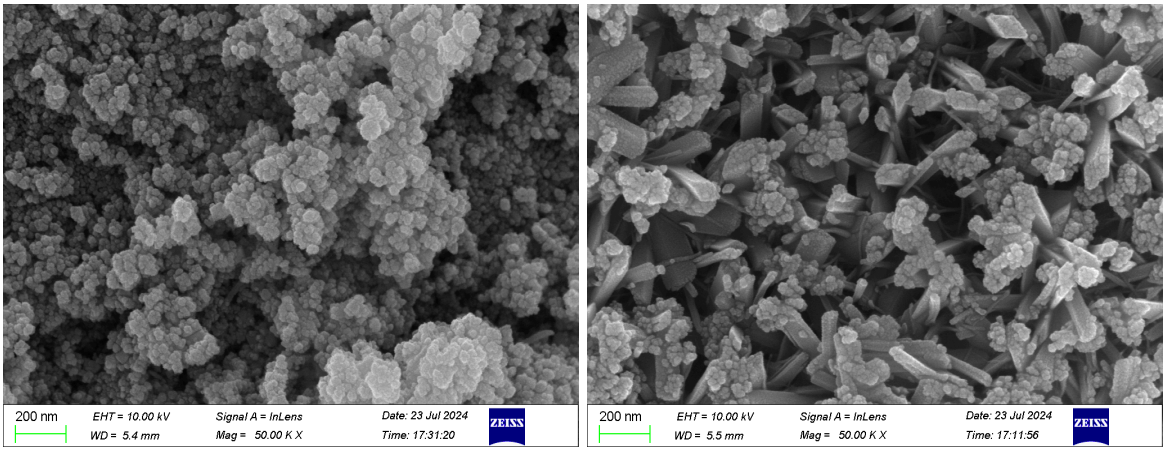

Figure 2. SEM images of (left) Fe_3O_4 nanoparticles (magnetite) and (right) YB-MNP.

Figure 2(left) shows Fe_3O_4 nanoparticles with an average size of about 20 nm forming clusters, while Figure 2(right) shows YB-MNP agglomerate under SEM, with Fe_3O_4 particles loaded onto the surface of the yeast biomass.

4.4 Point of zero charge (PZC) test

The pH_{PZC} of YB was observed to be 6.57 (Figure S4) while the pH_{PZC} of YB-MNP was observed to be 6.95 (Figure S5). These findings were similar to Bakkaloglu et al. (1998). This means that for pH > pH_{PZC}, the surface of the biomass had a negative charge, and for pH < pH_{PZC}, the surface of the biomass had a positive charge.

4.5 Removal of heavy metal ions with YB and YB-MNP

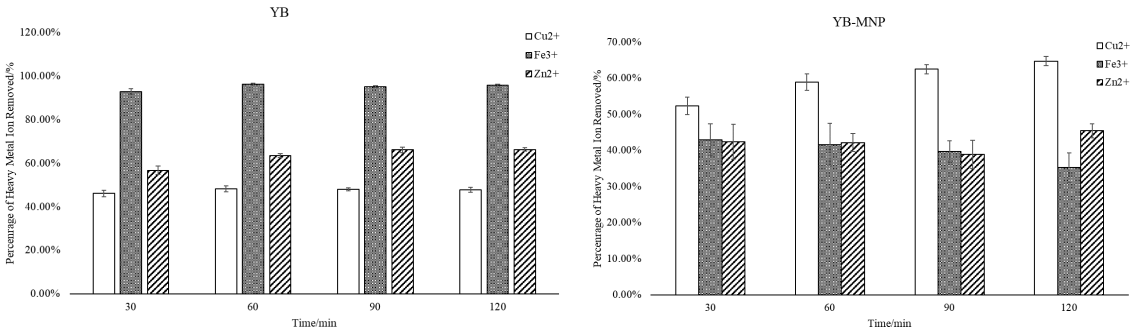

Figure 3. Graph of percentage heavy metal ions/% removed by YB (left) and YB-MNP (right) against time/min.

It was observed that maximum adsorption occurred within the first 30 minutes of contact, as shown in Figure 3. This was also observed by José et al. (2019). The rapid uptake of heavy metal ions and dyes could be attributed to the availability of binding sites present on the biomass surface as well as the biosorption of ions on the surfaces of each biomass (Tian et al., 2010).

Yeast cell walls are negatively charged due to the presence of hydroxyl, carboxylate and phosphoryl groups (Kregiel et al., 2012), as also shown in the YB FTIR spectra (Figure 1) with their respective peaks present. Electrostatic interactions allow positively charged heavy metal ions to bind to the negatively charged surface of the yeast.

Statistical analysis was obtained using the Mann-Whitney U Test on the final equilibrium concentration, where a p-value < 0.05 indicates statistical significance.

It was observed that YB significantly outperformed YB-MNP in the adsorption of Fe^{3+} ($p = 0.01193$), while slightly outperforming YB-MNP in the adsorption of Zn^{2+} ($p = 0.01193$). At the same time, YB-MNP slightly outperformed YB in the adsorption of Cu^{2+} ($p = 0.007937$).

Fe^{3+} adsorption was significantly favoured by YB, possibly due to the abundance of negatively charged sites on YB which decreases competition between H^+ ions and Fe^{3+} ions. This can be shown through YB's pH_{PZC} ($pH_{PZC} = 6.57$), where YB required extreme pH to deviate from its PZC. The absence or reduction of carboxylate and phosphoryl groups in YB-MNP, shown in its FTIR spectra in Figure 1, along with a wider range of pH that causes it to deviate from its PZC (Figure S5), means that YB-MNP is less effective at adsorbing cationic compounds.

	Heavy Metal Ion			Dye		
	Fe^{3+}	Cu^{2+}	Zn^{2+}	DR80	MB	MO
pH	2.39	4.85	5.40	6.58	4.94	5.73

Table 1. pH of Fe^{3+}, Cu^{2+}, Zn^{2+}, DR80, MB, and MO solutions.

Machado et al. (2010) found that the optimal pH for biosorption of Cu^{2+} and Zn^{2+} by yeast cells was close to 5 - 6. The pH of the Zn^{2+} solution falls within the optimal range while Cu^{2+} does not. This suggests that there are more properties of YB-MNP other than surface functional groups that participate in biosorption which allowed it to outperform YB in Cu^{2+} adsorption while underperforming in Zn^{2+} adsorption. Moreover, it is suggested by other researchers that biosorption has many mechanisms, ergo, surface adsorption is not the only mechanism in the removal of heavy metal ions from water (Brady & Tobin, 1995). For example, ion exchange is another biosorption mechanism that researchers have observed for both Cu^{2+} and Zn^{2+} (Brady & Duncan, 1994; Chen & Wang. 2007). The biosorption behaviour of heavy metal ions by YB and YB-MNP is complex and influenced by various factors, highlighting the need for further research to fully understand the different biosorption mechanisms involved in water purification.

4.6 Removal of dyes with YB and YB-MNP

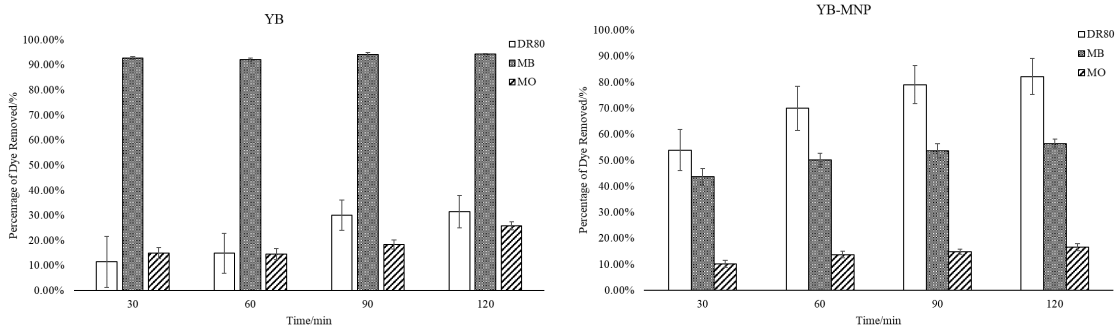

Figure 4. Graph of percentage of dye/% removed by YB (left) and YB-MNP (right) of direct red 80, methylene blue and methyl orange against time/min.

It was observed that YB-MNP significantly outperformed YB in the adsorption of direct red 80 ($p = 0.01587$). Meanwhile, YB significantly outperformed YB-MNP in the adsorption of

methylene blue ($p = 0.01141$) while there was significantly less adsorption of methyl orange by both YB and YB-MNP ($p = 0.01587$).

Direct red 80 (DR80) is an anionic dye. YB's more negatively charged surface will experience greater electrostatic repulsion with the negatively charged dye, as compared to the more positively charged surface of YB-MNP. Furthermore, $pH_{DR80} \approx pH_{PZC,\ YB}$ while $pH_{DR80} < pH_{PZC,\ YB\text{-}MNP}$. This makes the surface of YB-MNP more positively charged than YB, increasing electrostatic attraction between the surface of YB-MNP and DR80. This explains the affinity of DR80 to YB-MNP, as shown by the change in concentration of DR80 in Figure 4.

Methylene blue (MB), on the other hand, is a cationic dye. Like heavy metal ions, MB competes with H^+ ions in solution to bind to the surface of YB and YB-MNP. Furthermore, $(pH_{MB} - pH_{PZC,\ YB\text{-}MNP}) > (pH_{MB} - pH_{PZC,\ YB})$, making the surface of YB-MNP more positively charged than the surface of YB. Due to the lack of negatively charged sites on YB-MNP, more MB was adsorbed by YB than YB-MNP (Figure 4).

Compared to the other two dyes, methyl orange (MO) was significantly less adsorbed by both YB and YB-MNP compared to direct red 80, which is also an anionic dye. This could be explained by examining the structure of MO, as it has a single $-SO_3^-$ anionic group that provides a single site for electrostatic interaction with positively charged sites on the adsorbent surface, as compared to direct red 80, which has multiple $-SO_3^-$ anionic groups.

4.7 Removal of diesel by YB and YB-MNP

Diesel adsorption showed no significant difference between YB and YB-MNP ($p = 0.05556$), with varying rates of adsorption at different timesteps (Figure 5). Klis et al. (2002) found that S. cerevisiae has a cell wall predominantly composed of polysaccharides, proteins, and lipids, which feature hydrophilic functional groups such as -OH and $-NH_2$ groups as shown in the YB/YB-MNP spectra (Figure 1), making the surface of YB and YB-MNP hydrophilic. However, diesel is a hydrophobic substance. This polarity mismatch

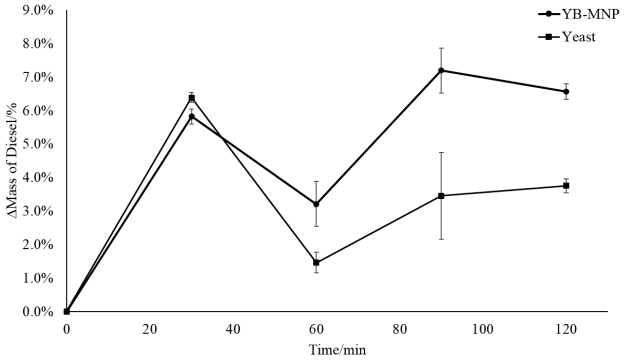

Figure 5. Graph of ΔMass of Diesel/% against time/min

between the hydrophilic surface of the biomass and the hydrophobic diesel results in poor adsorption efficiency, as the non-polar diesel molecules do not favourably interact with the polar functional groups on the biomass surface (Israelachvili, 2011).

4.8 Isotherm test

Langmuir and Freundlich constants and Langmuir R_L values from Figures S6 to S9 at C_e = 50 ppm were compared in the table below.

Biomass	Langmuir Constants				Freundlich Constants		
	K_b/mg/L	A_s/g/mg	R^2	R_L	n	K_f/L/mg	R^2
YB	-0.1196	-3.478	0.9875	-0.1996	1.676	2.878×10^{-6}	0.9582
YB-MNP	0.2704	19.84	0.9423	0.06854	0.6672	0.3290	0.9223

Table 2. Table representing Langmuir and Freundlich constants, R^2 and R_L for YB and YB-MNP.

From Table 2, it was deduced that the Langmuir model fitted both YB and YB-MNP better, as shown through its higher R^2 value. This means the biosorption process was based on monolayer adsorption, mostly on surface-active areas on YB and YB-MNP (Tian et al., 2010). Comparing R_L values, it was found that the adsorption of methylene blue by YB-MNP was more favourable than YB ($R_L > 0$ vs. $R_L < 0$ respectively).

Conclusion and Recommendations for Future Work

In this study, *S. Cerevisiae* yeast biomass (YB) was successfully grown, and magnetite (Fe_3O_4) was synthesised. The two were combined successfully to form a yeast-based magnetic bionanocomposite (YB-MNP). The synthesis was verified using an FTIR spectrophotometer and a scanning electron microscope. YB and YB-MNP could adsorb heavy metal ions, dyes, and diesel to varying degrees, depending on their properties, including surface charge. Surface charge was also explored by conducting point of zero charge tests. Depending on the adsorbate properties, YB and YB-MNP can outperform each other. The adsorption mechanisms of YB and YB-MNP were explored and both were found to fit the Langmuir isotherm model. No significant difference was found in diesel adsorption between YB and YB-MNP.

Future work can aim to further understand biosorption mechanisms and their differences in the biosorption of Cu^{2+} and Zn^{2+}. Furthermore, the effects of temperature and pH on contaminant

adsorption should be explored as they are important factors in the rate of contaminant adsorption (Tian et al., 2010). Isotherms of heavy metal ions and dyes other than methylene blue and diesel should also be explored to gain a better understanding of the adsorption mechanism of YB-MNP.

References

Allan, S. E., Smith, B. W., & Anderson, K. A. (2012). Impact of the Deepwater Horizon Oil Spill on Bioavailable Polycyclic Aromatic Hydrocarbons in Gulf of Mexico Coastal Waters. *Environmental Science & Technology, 46*(4), 2033–2039. https://doi.org/10.1021/es202942q

Bakkaloglu, I., Butter, T. J., Evison, L. M., Holland, F. S., & Hancock, I. C. (1998). Screening of various types biomass for removal and recovery of heavy metals (Zn, cu, ni) by biosorption, sedimentation and desorption. *Water Science and Technology, 38*(6), 269–277. https://doi.org/10.2166/wst.1998.0261

Bandera, G. (2023, January 18). *How Oil Spills Affect Humans and the Environment*. FairPlanet. https://www.fairplanet.org/story/how-oil-spills-affect-humans-and-the-environment/

Brady, D., & Duncan, J. R. (1994). Cation loss during accumulation of heavy metal cations by Saccharomyces cerevisiae. *Biotechnology Letters, 16*(5), 543–548. https://doi.org/10.1007/BF01023341

Brady, J. M., & Tobin, J. M. (1995). Binding of hard and soft metal ions to Rhizopus arrhizus biomass. *Enzyme and Microbial Technology, 17*(9), 791–796. https://doi.org/10.1016/0141-0229(95)00142-R

Carrilho, E. N. V. M., Ferreira, A. G., & Gilbert, T. R. (2002). Characterization of Sorption Sites on *Pilayella littoralis* and Metal Binding Assessment Using ^{113}Cd and ^{27}Al Nuclear Magnetic Resonance. *Environmental Science & Technology, 36*(9), 2003–2007. https://doi.org/10.1021/es0107834

Chen, C., & Wang, J.-L. (2007). Characteristics of Zn2+ biosorption by Saccharomyces cerevisiae. *Biomedical and Environmental Sciences: BES, 20*(6), 478–482. https://pubmed.ncbi.nlm.nih.gov/18348406/

Dahiya, S., Tripathi, R. M., & Hegde, A. G. (2008). Biosorption of heavy metals and radionuclide from aqueous solutions by pre-treated ARCA shell biomass. *Journal of Hazardous Materials, 150*(2), 376–386. https://doi.org/10.1016/j.jhazmat.2007.04.134

Israelachvili, J. N. (2011). Intermolecular and surface forces. Intermolecular and Surface Forces. https://doi.org/10.1016/c2009-0-21560-1

José, J. C., Abilio, T. E., Soares, B. C., Labuto, G., & Elma, C. (2019). Yeast-Based Magnetic Bionanocomposite for the Removal of Zn(II) in aqueous medium.

https://www.researchgate.net/publication/334749700_Yeast-Based_Magnetic_Bionanocomposite_for_the_Removal_of_ZnII_in_aqueous_medium

Karisma, D., Febrianto, G., & Mangindaan, D. (2017). Removal of dyes from textile wastewater by using nanofiltration polyetherimide membrane. *IOP Conference Series: Earth and Environmental Science, 109*, 012012. https://doi.org/10.1088/1755-1315/109/1/012012

Klis, F. M., Mol, P., Hellingwerf, K., & Brul, S. (2002). Dynamics of cell wall structure in Saccharomyces cerevisiae. *FEMS Microbiology Reviews, 26*(3), 239–256. https://doi.org/10.1111/j.1574-6976.2002.tb00613.x

Kregiel, D., Berlowska, J., & Ambroziak, W. (2012). Adhesion of yeast cells to different porous supports, stability of cell-carrier systems and formation of volatile by-products. *World Journal of Microbiology and Biotechnology, 28*(12), 3399–3408. https://doi.org/10.1007/s11274-012-1151-x

Labuto, G., Cardona, D. S., Bugan Debs, K., Ribeiro Imamura, A., Hipólito Bezerra, K. C., Neide Vasconcelos Martins Carrilho, E., & Haddad, P. S. (2018). Low-cost agroindustrial biomasses and ferromagnetic bionanocomposites to cleanup textile effluents. *DESALINATION AND WATER TREATMENT, 112*, 80–89. https://doi.org/10.5004/dwt.2018.21914

Liu, Q. (2020). Pollution and Treatment of Dye Waste-Water. *IOP Conference Series: Earth and Environmental Science, 514*(5), 052001. https://doi.org/10.1088/1755-1315/514/5/052001

Machado, M. D., Soares, E. V., & Soares, H. M. V. M. (2010). Removal of heavy metals using a brewer's yeast strain of Saccharomyces cerevisiae: Chemical speciation as a tool in the prediction and improving of treatment efficiency of real electroplating effluents. *Journal of Hazardous Materials, 180*(1–3), 347–353. https://doi.org/10.1016/j.jhazmat.2010.04.037

Nassar, N. N. (2010). Rapid removal and recovery of Pb(II) from wastewater by magnetic nanoadsorbents. *Journal of Hazardous Materials, 184*(1–3), 538–546. https://doi.org/10.1016/j.jhazmat.2010.08.069

Paul, J. H., Hollander, D., Coble, P., Daly, K. L., Murasko, S., English, D., Basso, J., Delaney, J., McDaniel, L., & Kovach, C. W. (2013). Toxicity and Mutagenicity of Gulf of Mexico Waters During and After the Deepwater Horizon Oil Spill. *Environmental Science & Technology, 47*(17), 9651–9659. https://doi.org/10.1021/es401761h

Qasem, N. A. A., Mohammed, R. H., & Lawal, D. U. (2021). Removal of heavy metal ions from wastewater: A comprehensive and critical review. *Npj Clean Water, 4*(1), 36. https://doi.org/10.1038/s41545-021-00127-0

Sadig, M., Alam, I. (1989). Metal concentrations in pearl oyster, *Pinctada radiata*, collected from Saudi Arabian Coast of the Arabian Gulf. *Bulletin of Environmental Contamination and Toxicology*, *42–42*(1), 111–118. https://doi.org/10.1007/BF01699211

Stokinger, H. E. (1984). A Review of World Literature Finds Iron Oxides Noncarcinogenic. *American Industrial Hygiene Association Journal, 45*(2), 127–133. https://doi.org/10.1080/15298668491399497

Tian, Y., Ji, C., Zhao, M., Xu, M., Zhang, Y., & Wang, R. (2010). Preparation and characterization of baker's yeast modified by nano-Fe3O4: Application of biosorption of methyl violet in aqueous solution. *Chemical Engineering Journal, 165*(2), 474–481. https://doi.org/10.1016/j.cej.2010.09.037

Yu, L., Hao, G., Gu, J., Zhou, S., Zhang, N., & Jiang, W. (2015). Fe_3O_4/PS magnetic nanoparticles: Synthesis, characterization and their application as sorbents of oil from waste water. *Journal of Magnetism and Magnetic Materials, 394*, 14–21. https://doi.org/10.1016/j.jmmm.2015.06.045

Appendix

Figure S1

Direct Red 80 Calibration Curve

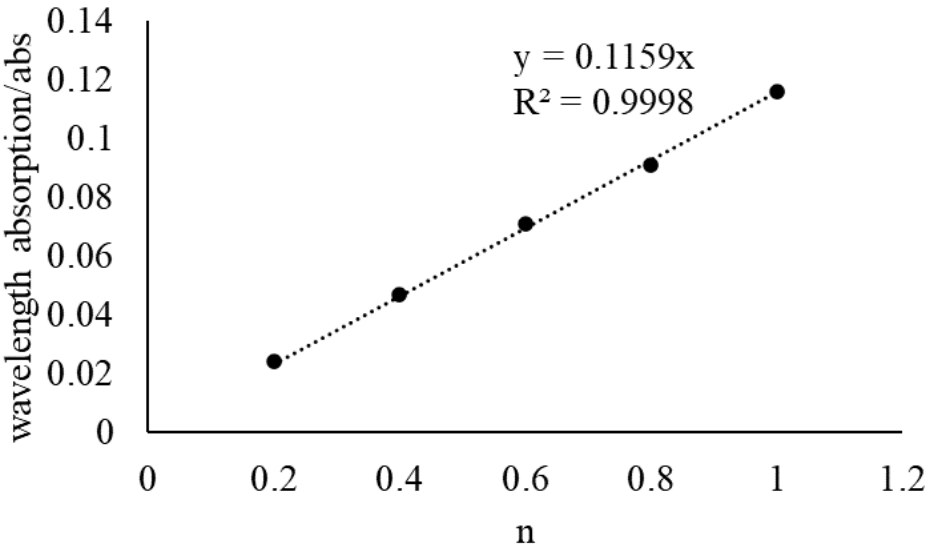

Note. Graph of wavelength absorption/abs of direct red 80 against n.

Figure S2

Methylene Blue Calibration Curve

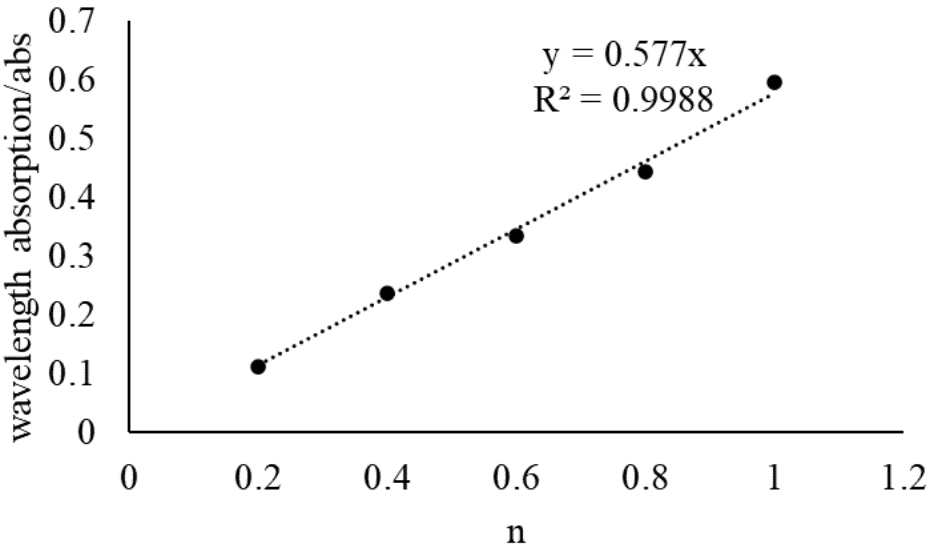

Note. Graph of wavelength absorption/abs of methylene blue against n.

Figure S3

Methyl Orange Calibration Curve

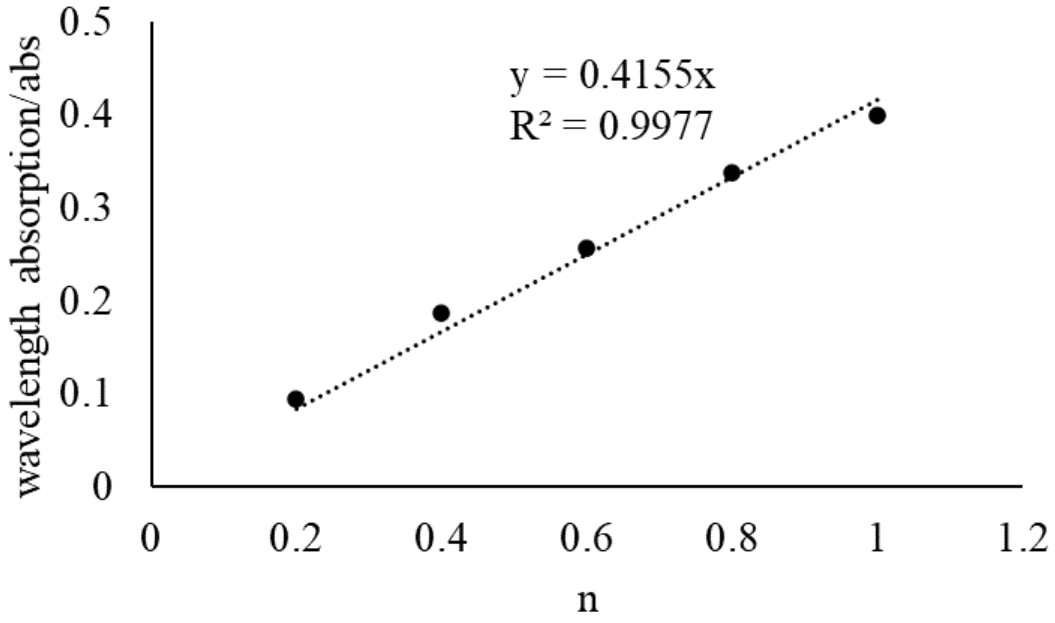

Note. Graph of wavelength absorption/abs of methyl orange against n.

Figure S4

Point of Zero Charge (PZC) of YB

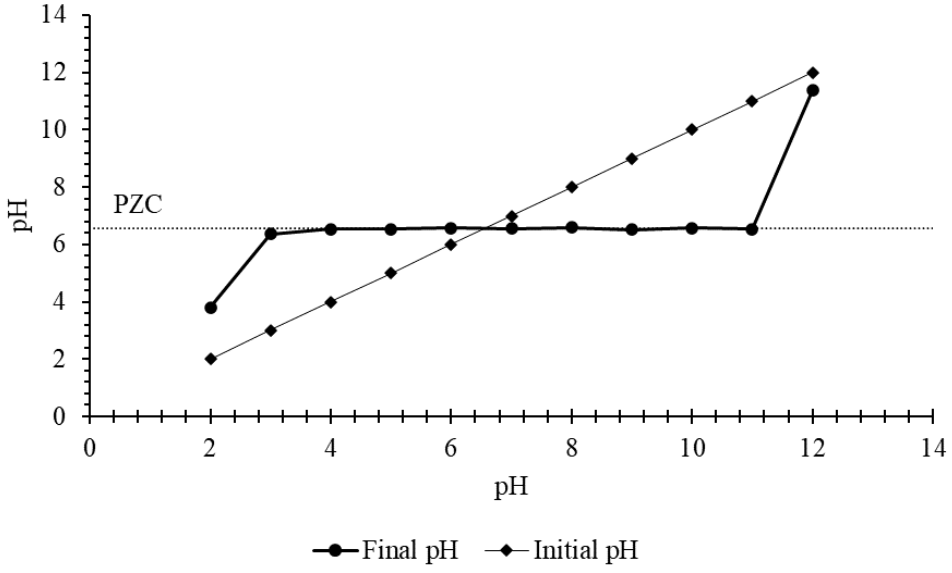

Note. Graph of final pH against initial pH and initial pH plotted on the same axis. PZC is also indicated.

Figure S5

Point of Zero Charge (PZC) of YB-MNP

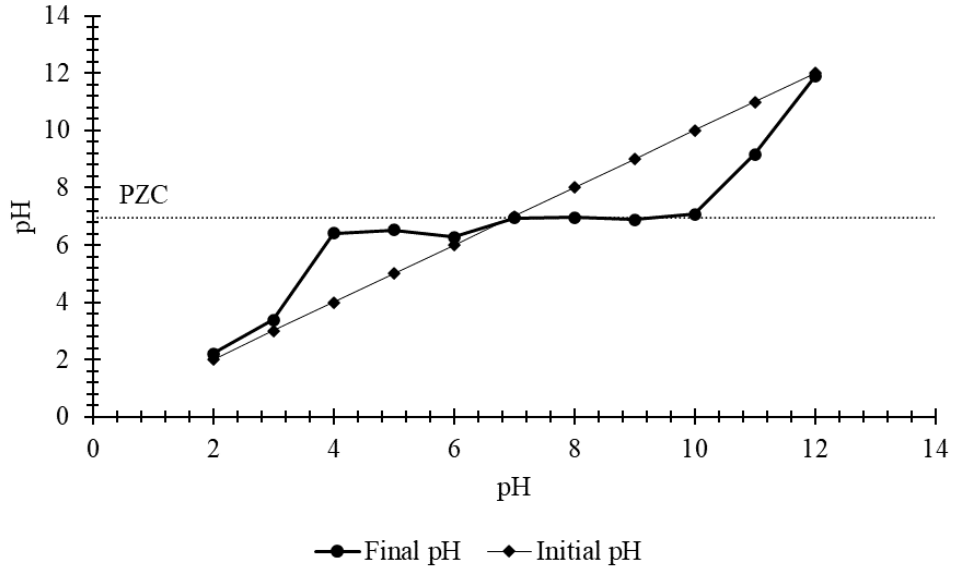

Note. Graph of final pH against initial pH and initial pH plotted on the same axis. PZC is also indicated.

Figure S6

Langmuir Isotherm of YB

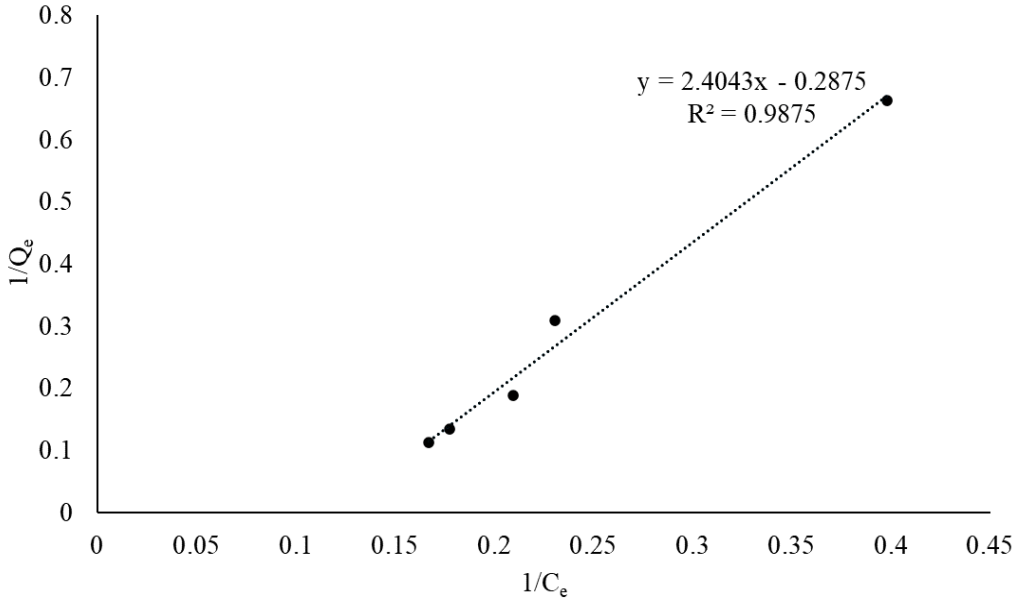

Note. Graph of $\frac{1}{Q_e}$ against $\frac{1}{C_e}$ of YB.

Figure S7

Freundlich Isotherm of YB

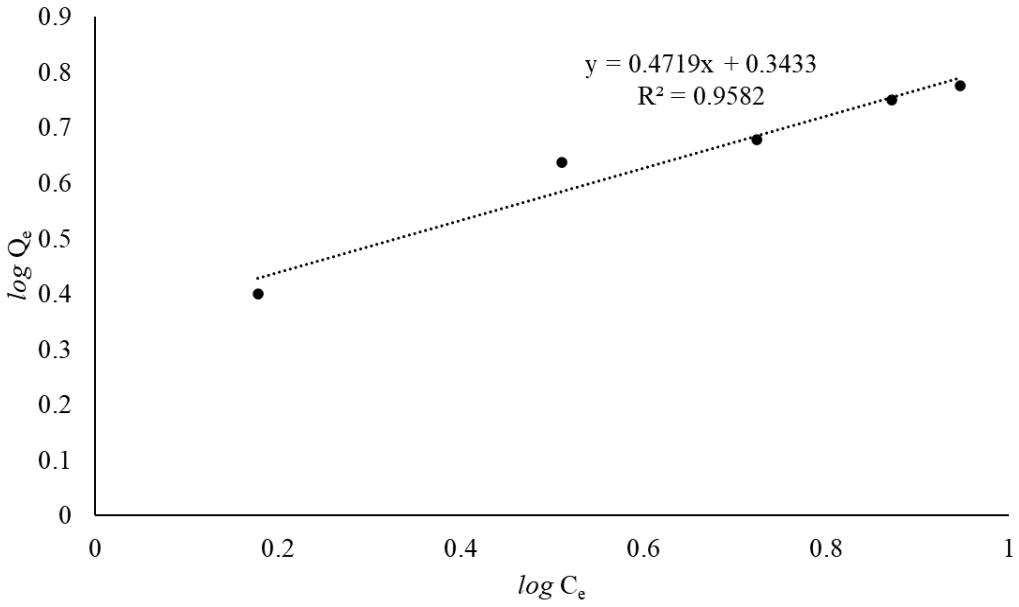

Note. Graph of *log* Q_e against *log* C_e of YB.

Figure S8

Langmuir Isotherm of YB-MNP

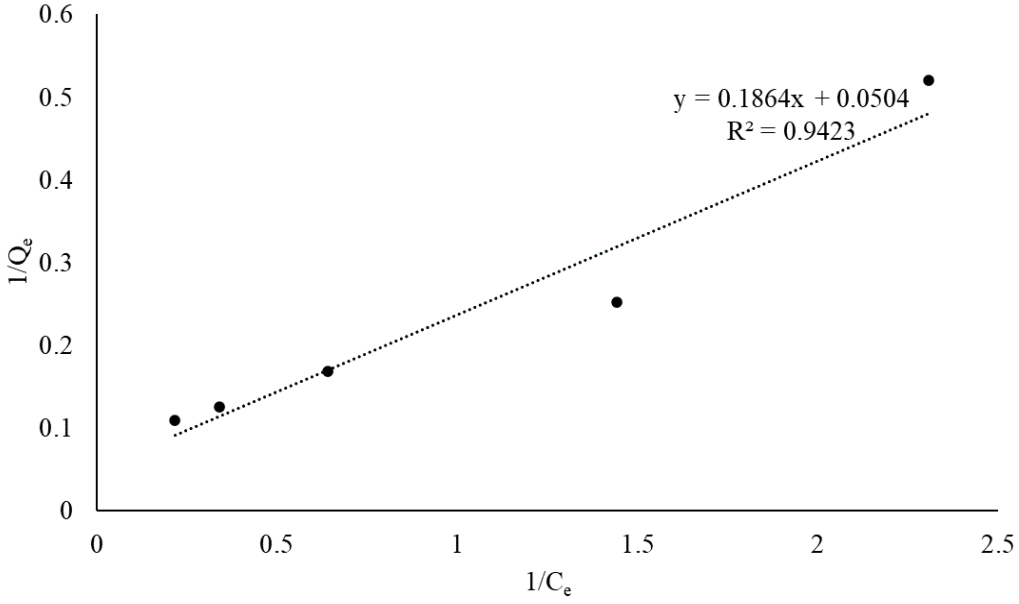

Note. Graph of $\frac{1}{Q_e}$ against $\frac{1}{C_e}$ of YB-MNP.

Figure S9

Freundlich Isotherm of YB-MNP

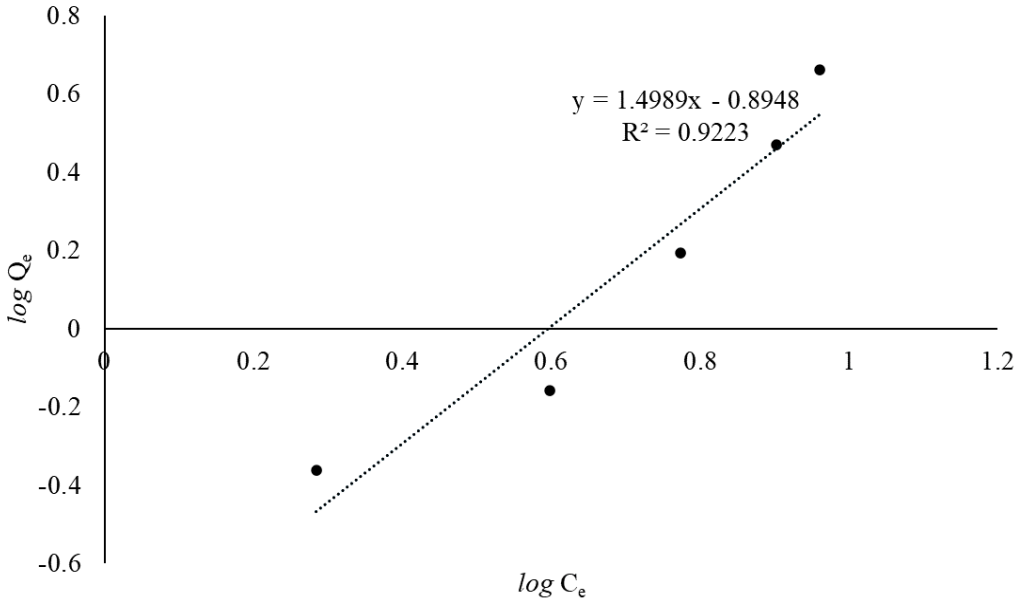

Note. Graph of *log* Q_e against *log* C_e of YB-MNP.